CHEMISTRY
A EUROPEAN JOURNAL

FULL PAPER

DOI: 10.1002/chem.200700398

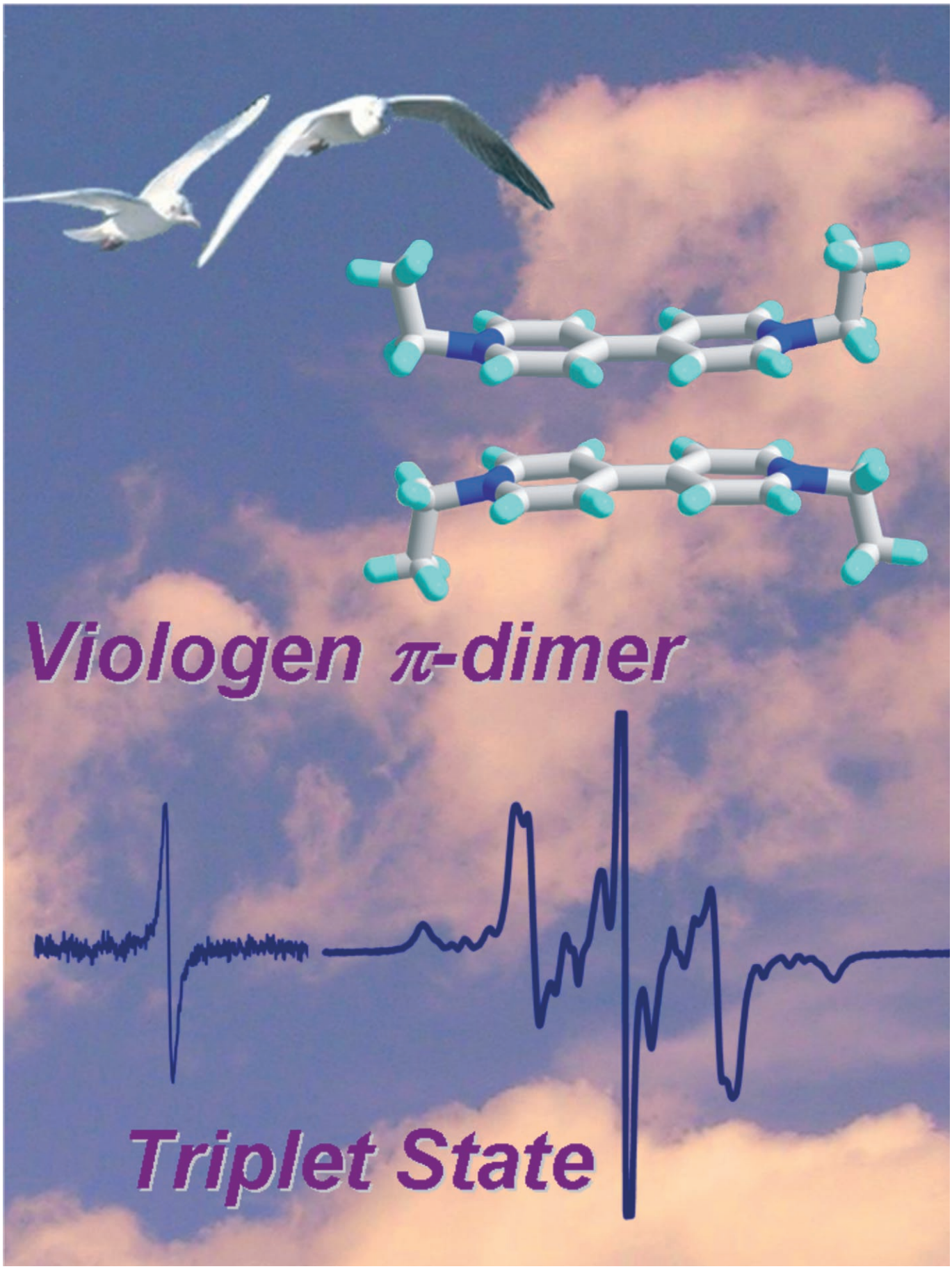

VIP

New Hybrid Semiconductor Materials Based on Viologen Salts of Bimetallic Fe–Pt and Fe–Au Carbonyl Clusters: First Structural Characterization of the Diradical π-Dimer of the Diethylviologen Monocation and EPR Evidence of its Triplet State

Cristina Femoni,[a] Maria Carmela Iapalucci,*[a] Giuliano Longoni,[a] Cristina Tiozzo,[a] Joanna Wolowska,[b] Stefano Zacchini,[a] and Enrico Zazzaroni[a]

Abstract: The synthesis, structure, spectroscopic characterization and electrical resistivity of the $[EtV]_2[Fe_4Pt(CO)_{16}]$, $[EtV][Fe_3Pt_3(CO)_{15}]\cdot THF$, $[EtV][Fe_4Au(CO)_{16}]_2\cdot 2THF$ (EtV = 1,1′-diethyl-4,4′-bipyridilium cation) and $[NEt_4]_2[Fe_4Au(CO)_{16}]$ is reported. The crystal structure of $[EtV]_2[Fe_4Pt(CO)_{16}]$ is based on infinite stacks of $[(EtV)^{\cdot+}]_2$ π-dimers rotated by 90° and isolated $[Fe_4Pt(CO)_{16}]^{2-}$ ions. Within each π-dimer, the $[EtV]^{\cdot+}$ radical ions are perfectly eclipsed and the distance between their mean planes is 3.275 Å. The EPR spectrum of the solid material at room temperature clearly indicates the presence of a significantly populated triplet state of the π-dimer, by showing signals both at $\Delta m = 1$ and $\Delta m = 2$. The solid-state structure of $[EtV][Fe_3Pt_3(CO)_{15}]\cdot THF$ is based on the ionic packing of $[EtV]^{2+}$ and $[Fe_3Pt_3(CO)_{15}]^{2-}$ ions, inferred from a comparison of their molecular parameters with literature data. Significant electron transfer could have been expected to give $[EtV]^{\cdot+}$ $[Fe_3Pt_3(CO)_{15}]^{\cdot-}$ on the basis of their formal redox potentials. In spite of their different stoichiometries, the structures of $[EtV][Fe_4Au(CO)_{16}]_2\cdot 2THF$ and $[NEt_4]_2[Fe_4Au(CO)_{16}]$ both contain an isomer of the monoanion $[Fe_4Au(CO)_{16}]^-$ in solution (previously characterized in the solid state as a $[NMe_3CH_2Ph]_2[Fe_4Au(CO)_{16}]Cl$ mixed salt). Resistivity measurements on pellets of powdered samples of the above compounds indicate that their tetrasubstituted ammonium salts, and complex $[EtV][Fe_4Au(CO)_{16}]_2\cdot 2THF$, largely behave as insulators. However, the $[EtV]_2[Fe_4Pt(CO)_{16}]$ and $[EtV][Fe_3Pt_3(CO)_{15}]\cdot THF$ samples respectively display resistivities 3 and 4 orders of magnitude less than those of their corresponding ammonium salts and could be classified as semiconductor materials.

Keywords: cluster compounds · EPR spectroscopy · metal carbonyls · semiconductors · viologens

Introduction

The field of charge- (CT) and electron-transfer (ET) salts that involve either organic molecules, coordination or organometallic compounds as components of molecular-based conductors contains a broad, rapidly expanding class of new materials that exhibit distinctive properties from those of isolated molecules or ions.[1]

Owing to the experimental observation that several homo- and hetero-metallic carbonyl clusters are multivalent or exhibit electrochemically reversible redox behaviour,[2,3] we became interested in the properties of their salts with redox-active countercations, with the hope of assembling a new class of molecule-based CT or ET salts belonging to the above categories of materials. The viologens (1,1′-disubstituted-4,4′-bipyridilium cations) appeared to be suitable candidates to act as redox-active countercations, because they feature 2+/1+ and 1+/0 redox changes, and formal potentials ($E°'$)[4] that are comparable with those of several metal carbonyl clusters. Moreover, the $E°'$ of their redox changes is tuneable as a function of the alkyl substituents and reac-

[a] Dr. C. Femoni, Dr. M. C. Iapalucci, Prof. G. Longoni, C. Tiozzo, Dr. S. Zacchini, E. Zazzaroni
Dipartimento di Chimica Fisica e Inorganica
Università di Bologna, Viale Risorgimento
4-40136 Bologna (Italy)
Fax: (+39) 051-209-3690
E-mail: iapa@ms.fci.unibo.it

[b] Dr. J. Wolowska
EPSRC Multi-Frequency EPR Centre, School of Chemistry
The University of Manchester, Oxford Road
Manchester M13 9PL (UK)

tion solvents.[4] Recently, we reported the synthesis and structure of the formerly uncharacterized $[Ag_{13}Fe_8(CO)_{32}]^{5-}$ pentaanion, as its ethylviologen radical monocation ($EtV^{\bullet+}$) salt.[5] As a further reason of interest, the crystal structure of this salt displayed stacks of ethylviologen radical cations, based on a sequence of A-B-A′-B′-A pentamers of twisted $[EtV]^{\bullet+}$ units, weakly interacting along the stack. The occurrence of CT and ET phenomena in solution and in the solid state was proposed on the basis of solution and solid-state spectroscopic observations.[5]

We now report, the results of our investigation of the synthesis and characterization of ethylviologen salts of some carbonyl clusters, $[Fe_4Pt(CO)_{16}]^{2-}$, $[Fe_3Pt_3(CO)_{15}]^{2-}$ and $[Fe_4Au(CO)_{16}]^{-}$. Further investigation has been undertaken to verify whether formation of contact ion pairs in these complexes could trigger CT or ET processes and induce conductor behaviour of these inorganic-organic hybrid salts. Fortuitously, we have isolated for the first time a perfectly eclipsed $[(EtV)^{\bullet+}]_2$ π-dimer, as its $[Fe_4Pt(CO)_{16}]^{2-}$ salt, that has triplet-state EPR signals that are clearly evident in the solid state at room temperature.

Results and Discussion

Synthesis and characterization of the $[EtV]_2[Fe_4Pt(CO)_{16}]$, $[EtV][Fe_3Pt_3(CO)_{15}]\cdot THF$ and $[EtV][Fe_4Au(CO)_{16}]_2\cdot 2THF$ salts: It has been reported that the $[Fe_4Pt(CO)_{16}]^{2-}$ ion[6] undergoes an irreversible one-electron oxidation to $[Fe_4Pt(CO)_{16}]^{\bullet-}$ with an $E^{\circ\prime}=+0.01$ V (against SCE and also in all following potentials). The backward response can only be observed at the highest scan rates, when reduction competes with the decomposition rate. As a result, a solution lifetime in the 0.1–1 s time range was assigned to the $[Fe_4Pt(CO)_{16}]^{\bullet-}$ ion.[7] On the basis of the formal potential of the $[EtV]^{2+}/[EtV]^{\bullet+}$ redox couple (≈ -0.39 V, in several organic solvents),[4,5] it appeared reasonable to think that the purported equilibrium in Equation (1) should not interfere with the preparation of a $[EtV][Fe_4Pt(CO)_{16}]$ salt, owing to a right-hand $\Delta E^{\circ\prime}=-0.4$ V and an expected value of $\approx 10^{-7}$ for its equilibrium constant in solution.

$$[Fe_4Pt(CO)_{16}]^{2-} + [EtV]^{2+} \rightleftharpoons [Fe_4Pt(CO)_{16}]^{\bullet-} + [EtV]^{\bullet+} \quad (1)$$

On the other hand, arbitrary assignment of a $\Delta E \approx -0.4$ V to a related equilibrium that occurs in the solid state might have given rise to a small amount of anion-cation electron transfer and, therefore, new salt-based conductor materials.[1]

Experimentally, treatment of alkali salts of the $[Fe_4Pt(CO)_{16}]^{2-}$ ion with $[EtV]I_2$ in a methanol suspension gives rise to a rather complicated reaction, which unexpectedly leads to a blue solution, which separates the $[EtV]_2[Fe_4Pt(CO)_{16}]$ salt as a microcrystalline material. Also formed in this solution are the already known $[Fe_3Pt_3(CO)_{15}]^{2-/\bullet-}$ [8] and $[Fe_3(CO)_{11}]^{\bullet-}$ cluster compounds.[9,10] The formation of the $[EtV]^{\bullet+}$ radical ion and the consequent separation of $[EtV]_2[Fe_4Pt(CO)_{16}]$ can only be derived from occurrence in solution of the equilibrium shown in Equation (1), even if its equilibrium constant is very small. Nevertheless, progressive shifting to the right may be a result of the ready and irreversible decomposition of $[Fe_4Pt(CO)_{16}]^{\bullet-}$ according to the reaction in Equation (2).

$$3\,[Fe_4Pt(CO)_{16}]^{\bullet-} \rightarrow [Fe_3Pt_3(CO)_{15}]^{\bullet-} + 2\,[Fe_3(CO)_{11}]^{\bullet-} + 2\,[Fe(CO)_5] + Fe + CO \quad (2)$$

In keeping with this suggestion, after filtering off the less-soluble $[EtV]_2[Fe_4Pt(CO)_{16}]$ salt from the reaction suspension, addition of water to the clear blue solution precipitates $[EtV][Fe_3Pt_3(CO)_{15}]\cdot THF$ (vide infra), $[EtV][HFe_3(CO)_{11}]$ and $[EtV][HFe_3(CO)_{11}]_2$ salts. The conversion of $[Fe_3(CO)_{11}]^{\bullet-}$ into $[HFe_3(CO)_{11}]^{-}$ by means of hydrogen-abstraction from solvent is known.[8]

The above decomposition products have also been observed upon oxidation of $[Fe_4Pt(CO)_{16}]^{2-}$ with other more powerful oxidizing agents such as tropylium tetrafluoroborate. In such a case, the oxidation of the starting compound to $[Fe_4Pt(CO)_{16}]^{\bullet-}$ is complete and readily affords the decomposition products of Equation (2). Protonic acids lead to the formation of the $[HFe_4Pt(CO)_{16}]^{-}$ hydride derivative, which is stable enough to be spectroscopically characterized ($\tilde{\nu}_{CO}$ at 2030 (s), 2010 (s), 1990 (s), 1950 (sh) cm^{-1}; $\delta_H = -14.8$ ppm; $J_{H-Pt}=1255$ Hz). $[HFe_4Pt(CO)_{16}]^{-}$ slowly decomposes on standing into a yet more complicated mixture of Fe–Pt, Fe and Pt carbonyl clusters, which also include some $[Pt_{3n}(CO)_{6n}]^{2-}$ species.[11]

The $[EtV]_2[Fe_4Pt(CO)_{16}]$ salt was crystallized from acetone and isopropyl alcohol mixtures and characterized by means of X-ray diffraction studies, IR and EPR spectroscopy (see later sections). Also the $[EtV][HFe_3(CO)_{11}]$ and $[EtV][HFe_3(CO)_{11}]_2$ salts have similarly been characterized and their structural data have been deposited. The structure of the $[HFe_3(CO)_{11}]^{-}$ cluster anion will not be described in detail owing to the lack of any significant additional features with respect to the previously reported structure.[12] Some relevant molecular parameters of the $[EtV]^{\bullet+}$ and $[EtV]^{2+}$ ions are given in Table 1, for sake of comparison.

On the basis of the formal potential of the $[EtV]^{2+}/[EtV]^{\bullet+}$ (≈ -0.39 V, in several organic solvents) and $[Fe_3Pt_3(CO)_{15}]^{2-}/[Fe_3Pt_3(CO)_{15}]^{\bullet-}$ (≈ -0.31 V) redox couples,[13] the equilibrium in Equation (3) should exhibit a much greater constant (≈ 1) than the equilibrium in Equation (1).

$$[Fe_3Pt_3(CO)_{15}]^{2-} + [EtV]^{2+} \rightleftharpoons [Fe_3Pt_3(CO)_{15}]^{\bullet-} + [EtV]^{\bullet+} \quad (3)$$

In keeping with this suggestion, solutions of $Na_2[Fe_3Pt_3(CO)_{15}]$ in methanol turn deep blue upon addition of $[EtV]I_2$ owing to formation of the $[EtV]^{\bullet+}$ radical. Accordingly, IR and EPR monitoring of the solution shows the presence of a mixture of $[Fe_3Pt_3(CO)_{15}]^{2-/\bullet-}$ cluster compounds and the $[EtV]^{\bullet+}$ radical ion. The [EtV]-

$[Fe_3Pt_3(CO)_{15}]$·THF salt has been precipitated by the addition of water and crystallized from a THF–toluene mixture. The salt has been characterized by means of X-ray diffraction studies, IR and EPR spectroscopy (see later sections).

The $[EtV][Fe_4Au(CO)_{16}]_2$·2THF salt has been obtained by using cation metathesis of its sodium salt in methanol, prepared by using literature methods,[14,15] with an excess of aqueous $[EtV]I_2$. The salt has been crystallized from a THF–toluene mixture and is soluble in THF, acetone and acetonitrile, to give dark-green solutions, which are EPR silent and display infrared carbonyl absorptions perfectly matching those of the $[Fe_4Au(CO)_{16}]^-$ ion as a tetrasubstituted ammonium salt.[14,15]

Attempts to isolate a 1:1 $[EtV]^{\bullet+}$ salt of the $[Fe_4Au(CO)_{16}]^-$ ion have been unsuccessful. Addition of an $[EtV]^{\bullet+}$ solution, prepared by reducing $[EtV]I_2$ with Zn metal,[4] led to precipitation of some $[EtV][Fe_4Au(CO)_{16}]_2$·2THF and various decomposition products. That probably stems from occurrence in solution the following equilibrium seen in Equation (4).

$$[Fe_4Au(CO)_{16}]^- + [EtV]^{\bullet+} \rightleftharpoons [Fe_4Au(CO)_{16}]^{2\bullet-} + [EtV]^{2+} \quad (4)$$

Taking as reference, the formal potentials of the relative redox couples,[14] the equilibrium in Equation (4) should have a very small equilibrium constant and be substantially coincident with the equilibrium constant of Equation (1). It may be conjectured, that the limited stability of $[Fe_4Au(CO)_{16}]^{2\bullet-}$, which decomposes into yet unidentified products, favours a partial shift to the right of the equilibrium in Equation (4), to produce enough of the $[EtV]^{2+}$ ion to reach the solubility product of the $[EtV][Fe_4Au(CO)_{16}]_2$·2THF salt.

The structure of the $[EtV]_2[Fe_4Pt(CO)_{16}]$ salt: The structure of the $[EtV]_2[Fe_4Pt(CO)_{16}]$ salt is made up of packed of $[Fe_4Pt(CO)_{16}]^{2-}$ ions and $[(EtV)^{\bullet+}]_2$ π-dimer ions. A few O···H contacts between the oxygen atoms of the carbonyl groups and the hydrogen atoms bound to the carbon atoms of the aromatic rings of the cation π-dimers are slightly shorter than normal van der Waals contacts. By far, the most notable features are that, within each dimer, the $[EtV]^{\bullet+}$ moieties are perfectly eclipsed (see Figure 1 top, which also reports the general numbering scheme) and display mean plane distance of 3.275 Å. This is possible since both $[EtV]^{\bullet+}$ radical ions exhibit a *cis* conformation of their ethyl groups. Additionaly, there are infinite stacks of dimers present, rotated by ≈90° and slightly tilted (Figure 1 bottom, interdimer distance ≈4.15 Å).

The monocationic nature of each ethylviologen unit is confirmed by analysis of the interannular C–C and intraring C–C and C–N bond lengths (for a more detailed discussion see section on the structure of the $[EtV][Fe_3Pt_3(CO)_{12}]$·THF salt below and Table 1).

The tendency of some organic radicals to give rise to π-bonded, rather than σ-bonded, dimeric products both in solution and in the solid state is well documented.[16] Dimers or more complex aggregates have also been suggested in viologen radical chemistry to explain, for instance, the colour changes on changing the solution solvent from CH_2Cl_2 or CH_3CN (blue) to water (purple).[4] A dimer of the methylviologen radical monocation has been recently trapped in a cucurbit[8]uril cavitand.[17] Nonetheless, to the best of our knowledge, none of these dimers have been isolated and structurally and spectroscopically characterized. The only

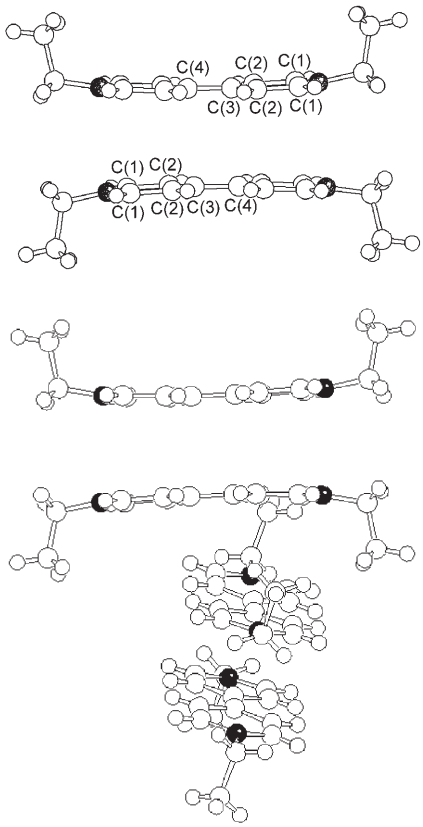

Figure 1. Top: The $[(EtV)^{\bullet+}]_2$ π-dimer (the numbering scheme refers to Table 1). Bottom: The stack of twisted and tilted π-dimers present in the solid-state structure of $[EtV]_2[Fe_4Pt(CO)_{16}]$.

Table 1. C–C and C–N average bond lengths [Å] and skew angles [°] for H-, methyl- and ethyl-disubstituted viologens cations in their miscellaneous redox forms.

Compound	C1–C2	C2–C3	C3–C4	N1–C1	Skew angle	Ref.
$[HV]^{2+}[PtCl_6]^{2-}$	1.385	1.399	1.474	1.336	40.65	[29]
$[HV]^{2+}[PtCl_4]^{2-}$	1.371	1.377	1.496	1.325	0.44	[29]
$[MeV]^{2+}[(Cl)^-]_2$	1.40	1.40	1.45	1.34	50	[4]
$[MeV]^{\bullet+}[PF_6]^-$	1.34	1.42	1.42	1.37	6–11	[18]
MV^0	1.32	1.46	1.36	1.38	0	[18]
$[EtV]^{2+}[Fe_3Pt_3(CO)_{15}]^{2-}$	1.370	1.392	1.481	1.337	18.7	[a]
$[EtV]^{2+}[(Fe_4Au(CO)_{16})^-]_2$	1.359	1.384	1.470	1.330	0	[a]
$[EtV]^{2+}[(HFe_3(CO)_{11})^-]_2$	1.359	1.391	1.486	1.338	0	[a]
$[(EtV)^{\bullet+}]_5[Ag_{13}Fe_8(CO)_{32}]^{5-}$	1.32	1.42	1.44	1.36	0–4	[5]
$[(EtV)^{\bullet+}]_2[Fe_4Pt(CO)_{16}]^{2-}$	1.353	1.426	1.421	1.355	0.3	[a]
$[EtV]^{\bullet+}[HFe_3(CO)_{11}]^-$	1.359	1.426	1.421	1.356	5.7	[a]

[a] This work.

structures known to date for viologen radical monocations are those of $[(EtV)^{\bullet+}]_5[Ag_{13}Fe_8(CO)_{32}]$[5] and $[MeV]^{\bullet+}[PF_6]^-$ (MeV = 1,1′-dimethyl-4,4′-bipyridilium cation).[18] In the former, the $[EtV]^{\bullet+}$ ions are arranged in stacks that have an interplane distance of ≈3.2 Å (shorter C–C contacts 3.32 Å) and torsion angles between consecutive units of ≈90°. Similarly, the $[MeV]^{\bullet+}$ ions of the latter are assembled in infinite stacks that have an intermolecular distance of 3.29 Å and a torsion angle between consecutive units of 37°. Along the stack an ordered sequence of pairs of methyl viologen units is present. The two units making a pair, feature slightly different molecular parameters, owing to the $[MeV]^{\bullet+}/[MeV]^{\bullet+}$ $\rightleftarrows[MeV]^{2+}/[MeV]^0$ charge-transfer resonance.[18]

In contrast, in the case of $[EtV]_2[Fe_4Pt(CO)_{16}]$, the $[(EtV)^{\bullet+}]_2$ π-dimers are separated, since the methyl groups are directed outwards from the molecular planes and keep the other dimers slightly further apart. The two $[EtV]^{\bullet+}$ units within each π-dimer are perfectly eclipsed and display identical molecular parameters. The monocationic moieties are not perfectly planar, since the nitrogen atoms are slightly shifted from the molecular plane. As a result, the intermolecular N···N contact (3.390(2) Å) is slightly longer than the intermolecular distance between the ipso-carbon atoms (3.176(2) Å). Therefore, to our knowledge, the $[EtV]_2[Fe_4Pt(CO)_{16}]$ provides the first proof of the possible existence of a viologen long-bonded π-dimer of radical monocations and provides the unique opportunity to investigate its nature.

The $[Fe_4Pt(CO)_{16}]^{2-}$ ion closely resembles one previously characterized as a $[NMe_3CH_2Ph]^+$ salt;[6] only the carbonyl stereochemistry is slightly different. A comparison between the most significant bond contacts is reported in Table 2.

Table 2. Comparison between anion bond lengths [Å] in $[EtV]_2[Fe_4Pt(CO)_{16}]$ and $[NMe_3CH_2Ph]_2[Fe_4Pt(CO)_{16}]$.[a]

	$[EtV]_2[Fe_4Pt(CO)_{16}]$	$[NMe_3CH_2Ph]_2[Fe_4Pt(CO)_{16}]$
Pt–Fe	2.597–2.623	2.601
Fe–Fe	2.692	2.708
Fe–C_t	1.789	1.765
C_t–O	1.146	1.15
Fe–C_b	1.839	1.814
C_b–O	1.167	1.16
Pt–C_b	2.155, 2.398	2.285

[a] C_t: terminal carbon; C_b: bridging carbon.

The complex $[NMe_3CH_2Ph]_2[Fe_4Pt(CO)_{16}]$ has one CO ligand per $Fe(CO)_4$ group that is bent toward the central Pt atom, which displays a square-planar coordination with four Fe atoms and a superimposed tetrahedral coordination that has four weakly interacting carbonyl groups. The Pt–C distances (av. 2.285 Å) are rather long and the Pt–CO interaction can, hereafter, be described as incipient bridges. Conversely, two of the above incipient CO bridges in $[EtV]_2[Fe_4Pt(CO)_{16}]$ (Figure 2) might be classified as asymmetric bridging ligands since they display significantly shorter Pt–C distances (av. 2.155 Å), increased Fe–C distances (av. 1.839 vs. 1.814 Å) and Fe–C–O and Pt–C–O angles of ≈155 and 123°, respectively. Almost as a consequence, the other two CO ligands are moved equally apart from Pt (Pt–C av. 2.398 Å), which obtains a distorted octahedral coordination. Notably, this affects the Fe–Pt interactions: the two Fe–Pt contacts supported by the asymmetric CO bridges are slightly longer than the unsupported ones (av. 2.623 vs. 2.597 Å). In general, CO bridges shorten the spanned M–M bonds.[19] Interestingly, the nujol mull IR spectrum of $[EtV]_2[Fe_4Pt(CO)_{16}]$ displays a carbonyl absorption in the bridging region ($\tilde{\nu}_{CO}$ at 1792 cm^{-1}), which is absent in solution, as well as in the solid-state spectrum of its tetrasubstituted ammonium salts.

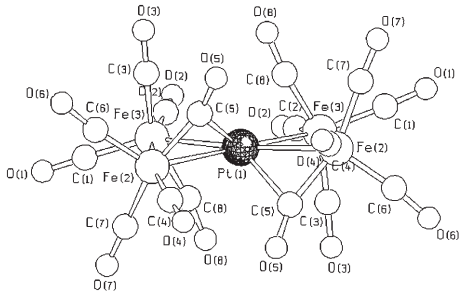

Figure 2. The structure of the $[Fe_4Pt(CO)_{16}]^{2-}$ ion.

The EPR spectrum of the $[EtV]_2[Fe_4Pt(CO)_{16}]$ salt: The crystals of $[EtV]_2[Fe_4Pt(CO)_{16}]$ are soluble in acetone and acetonitrile, sparingly soluble in alcohols and THF, and insoluble in nonpolar solvents. Solutions of the salt in acetonitrile are green-blue and show infrared carbonyl absorptions at 2022 (w), 1991 (s), 1977 (s), 1937 (mw), 1916 (w) and 1840 (w, broad) cm^{-1} identical to those of other tetrasubstituted ammonium salts of the $[Fe_4Pt(CO)_{16}]^{2-}$ ion.[6] The EPR spectrum of this solution at 298 K shows a signal of the $[EtV]^{\bullet+}$ radical ion with only a partially resolved hyperfine structure (Figure 3a). Moreover, the EPR spectrum of the glass, obtained by freezing the above solution at 100 K, only shows the isotropic signal at ≈3380 G of the solvated $[EtV]^{\bullet+}$ radical ion. Therefore, the IR and EPR spectra rule out persistence in solution of the above diradical π-dimers, as well as contact cation–anion pairs and occurrence of anion-to-cation CT.

The EPR of a polycrystalline sample of the $[(EtV)^{\bullet+}]_2[Fe_4Pt(CO)_{16}]$ salt displays a complicated pattern (Figure 3b). The starred peaks are a result of incomplete randomization of the crystals and disappear on progressive grinding of the sample. Nevertheless, the spectrum is quite different from the isotropic signal observed in the above glassy samples and $[(EtV)^{\bullet+}]_5[Ag_{13}Fe_8(CO)_{32}]$,[5] as well as the anisotropic signal of crystalline $[MeV]^{\bullet+}[PF_6]$.[18] The signal is ≈300 G wide and centred at the typical field of viologen radicals. The observed pattern clearly arises from a significantly-populated triplet state of the $[EtV]^{\bullet+}\cdots[EtV]^{\bullet+}$ π-dimer and separated $[EtV]^{\bullet+}$ radical. The latter is responsible of the central most intense signal. The triplet state of

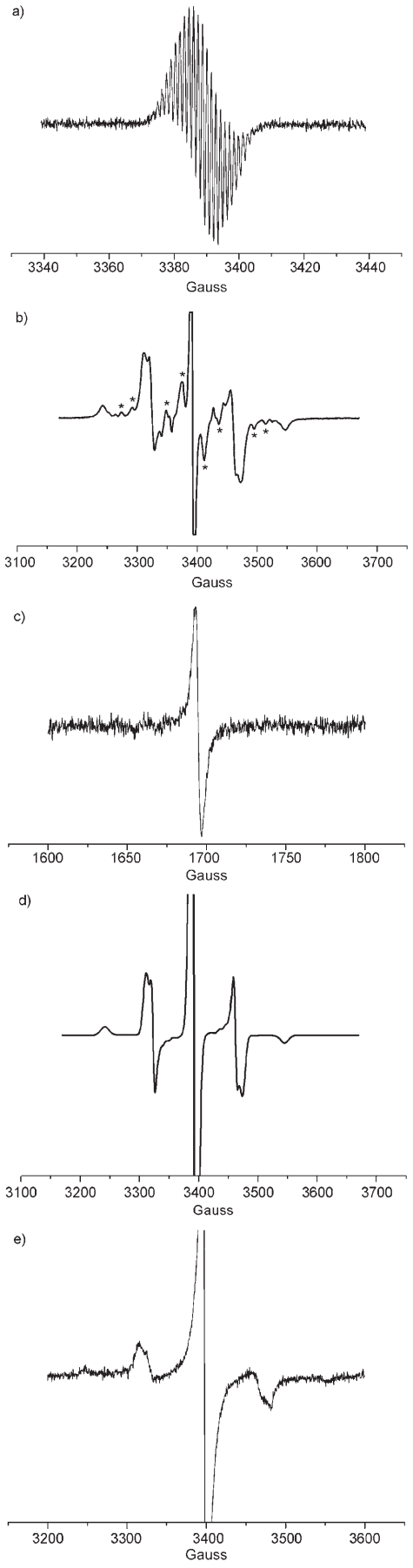

Figure 3. a) The experimental EPR spectra of $[EtV]_2[Fe_4Pt(CO)_{16}]$ in acetonitrile, b) as a solid crystalline sample at $\Delta m=1$ and at c) $\Delta m=2$, d) simulation of the spectrum with parameters reported in the text, and e) sample after repeated grindings.

the $[EtV]^{\bullet+}\cdots[EtV]^{\bullet+}$ π-dimer is implemented by a weak feature at ≈1690 G (Figure 3c) corresponding to the forbidden transition with $\Delta m=2$.

Analysis of the spectrum allows to deduce the following zero-field splitting parameters $|D|=141.0\times10^{-4}\,cm^{-1}$ and $|E|=4.0\times10^{-4}\,cm^{-1}$. Note that the midpoints of the pairs of resonances coincide, this would indicate that the isotropy of the g factor ($g_x=g_y=g_z=2.00$). Simulation of the EPR spectrum of the $[EtV]^{\bullet+}\cdots[EtV]^{\bullet+}$ π-dimer on the basis of the above zero-field parameters is shown in Figure 3d. The value of $|D|$ enables a rough estimation of the average distance between the two radical centres. Using the point-dipole approximation, from the equation $D=\beta^2g^2r^{-3}$ an average distance of ≈3.9 Å can be estimated, which is in fair agreement with the interplane distance between the two [EtV] moieties of the π-dimer.

Cooling of the sample to 100 K causes the almost complete disappearance of the triplet signal, which can be restored back to its original intensity upon warming to room temperature. This would indicate that the triplet is an excited state with respect to the singlet state. The thermal behaviour of the $[EtV]^{\bullet+}\cdots[EtV]^{\bullet+}$ π-dimer is comparable to that of the recently reported thiazyl π-dimer.[20]

The triplet EPR signals of diradical σ-dimers derived, for instance, from dimethylenecyclobutadiene, highly-hindered silacyclobutadienes and 1-methyl-2-(carbomethoxy)pyridine, both in solution or glasses, have been reported.[21,22,23] The only previously documented triplet state of a diradical π-dimer that we are aware of is the above thiazyl derivative,[20] whereas the intramolecular π-dimer of verdazyl moieties in the 1,1′-bis(verdazyl)ferrocene biradical,[24] or the *m*-phenylenediamine radical cations linked by twisted benzenes (tetraazacyclophane),[25] are known.

It seems reasonable to suggest that strongly interacting, tight π-dimers should exhibit a singlet state. As the intermolecular distance increases and the interaction weakens, increasingly populated triplet states could be expected. Beyond a certain elongation of the intermolecular distance the nature of a single $[EtV]^{\bullet+}$ radical ion should show up. In this regard, it is significant that previously reported cationic, anionic or neutral π-dimers featuring shorter interunit separations display singlet ground states [e.g., 2.87 ($TCNE^{\bullet+}$; tetracyanoethylene), 2.90 (cloranil radical anion), 2.90 ($DDQ^{\bullet-}$; dichlorodicyanoquinone), 3.05 ($OMB^{\bullet+}$; octamethylbiphenylene), 3.2 ($TCNQ^{\bullet-}$; tetracyanoquinodimethane), and 3.22 Å ($Phen^{\bullet}$; phenalene)].[16]

The structure of the $[EtV][Fe_3Pt_3(CO)_{15}]\cdot THF$ salt: The unit cell of $[EtV][Fe_3Pt_3(CO)_{15}]\cdot THF$ contains one $[Fe_3Pt_3(CO)_{15}]^{2-}$ ion, one $[EtV]^{2+}$ ion and one THF molecule. The packing of these ions is based on layers composed of rows of anions alternated by rows of cations and THF

molecules. Adjacent layers are in a staggered orientation and, therefore, each row of anions is completely surrounded by rows of cations and THF molecules. The shortest nonbonding anion–cation contacts are between the O atoms of the axial carbonyl groups bound to Fe and some H, C and N atoms of the cations (O···H 2.47–2.53, O···C 3.06–3.22, O···N 3.02 Å). Both the anion and the cation are nonplanar. Only the structure of $[Fe_3Pt_3(CO)_{15}]^{2-}$ is shown in Figure 4 with

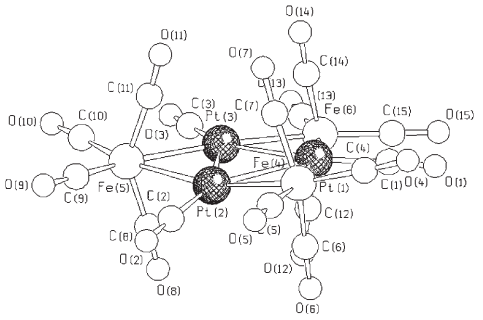

Figure 4. The structure of the $[Fe_3Pt_3(CO)_{15}]^{2-}$ ion.

its labelling. The three Fe atoms and Pt(1) of the dianion lay in the same plane, whereas Pt(2) and Pt(3) are located slightly below (0.321 Å) and above (0.075 Å) this plane, respectively. This type of deformation has not been previously observed in any of the clusters of the $[Fe_3Pt_3(CO)_{16}]^{n-}$ ($n=$ 0, 1, 2) series.[8,26] A dianionic nature can be unambiguously attributed to $[Fe_3Pt_3(CO)_{15}]^{2-}$ by a comparison of its average Pt–Pt and Pt–Fe bond lengths with those of the previously characterized $[Fe_3Pt_3(CO)_{16}]^{n-}$ ($n=0$, 1, 2) species.[8,26] As shown in Table 3, the distances displayed by the anion present in the crystal structure of $[EtV][Fe_3Pt_3(CO)_{15}]\cdot THF$ are almost identical to those of its corresponding $[NBu_4]_2[Fe_3Pt_3(CO)_{15}]$ salt.[8] Accordingly, the infrared carbonyl absorptions in the nujol mull spectrum fall below 2000 cm^{-1}. Therefore, it can be concluded that the charge of the cluster present in this ethylviologen salt is primarily −2. On the basis of the stoichiometry, the salt has to be formulated as $[EtV]^{2+}[Fe_3Pt_3(CO)_{15}]^{2-}\cdot THF$.

Table 3. M–M distances [Å] for the clusters $[Fe_3Pt_3(CO)_{15}]^{n-}$ ($n=0$, 1, 2).

Anion	Cation	Pt-Pt	Pt-Fe	Ref
$[Fe_3Pt_3(CO)_{15}]$	–	2.590(2)	2.578(2)	[26]
$[Fe_3Pt_3(CO)_{15}]^-$	$[NMe_3CH_2Ph]^+$	2.656(1)	2.587(4)	[8]
$[Fe_3Pt_3(CO)_{15}]^{2-}$	$[NBu_4]^+$	2.750(1)	2.596(4)	[8]
$[Fe_3Pt_3(CO)_{15}]^{2-}$	$[EtV]^{2+}$	2.753(1)	2.594(2)	[a]

[a] This work.

In spite of a skew angle between the rings of ≈18.7°, the +2 charge of the 1,1′-diethyl-4,4′-bipyridilium is made necessary by electroneutrality and is clearly pointed out by the individual values of its interannular C–C and intra-ring C–C and C–N bond lengths. Indeed, it has previously been suggested that the charge of viologen cations could be unraveled by the skew angle between the rings, because quantum-mechanical calculations[27,28] have pointed out that the viologen dication exhibits an energy minimum for a skew angle of ≈44.7°, whereas a minimum in the range 11.9–13.6° has been suggested for the radical monocation in the absence of any external force (gas phase). The resultant experimental solid-state skew angles are significantly smaller than 45° and have often been taken as an indication of charge transfer from the anion to the cation.[4] Analysis of the crystal structures of several viologen salts of miscellaneous counter anions reported in the literature,[4,5,18,29] leads to the suggestion that the skew angles of dicationic species may decrease from 40 to 0°, as a consequence of intermolecular interactions or packing efficiency rather than as a result of charge transfer. Indeed, CT phenomena in $[EtV]^{2+}$ $[PtCl_6]^{2-}$ appear rather unlikely. Nevertheless, the viologen dication displays a skew angle of about 10°.[29]

Both theoretical and experimental data agree that the reduction of a viologen dication progressively destroys its aromaticity, and that the monocation and the neutral viologen progressively behave as a polyene with alternating single and double bonds.[18] Following that and, as previously concluded by J. K. Kochi,[18] the interannular C–C and intra-ring C–C and C–N distances are much more diagnostic of the charge of the viologens than the skew angles. The relevant bond lengths observed for the ethylviologen in $[EtV][Fe_3Pt_3(CO)_{15}]\cdot THF$ and those of other H-, Me- and Et-disubstituted V^{2+} and $V^{\cdot+}$ salts are collected in Table 1. The comparison clearly indicates that $[EtV]^{2+}$ ions are primarily present in the unit cell of $[EtV][Fe_3Pt_3(CO)_{15}]\cdot THF$.

The fact that the bis-charged cation and anion are primarily present in the $[EtV][Fe_3Pt_3(CO)_{15}]\cdot THF$ salt was unexpected, because, as discussed above, the solution redox potentials of the $[EtV]^{2+}/[EtV]^{\cdot+}$ and $[Fe_3Pt_3(CO)_{15}]^{-}/[Fe_3Pt_3(CO)_{15}]^{2-}$ redox couples suggest that the constant of the equilibrium in Equation (3) in solution should be close to 1. Accordingly, comparable amounts of $[Fe_3Pt_3(CO)_{15}]^{\cdot-}$ and $[Fe_3Pt_3(CO)_{15}]^{2-}$ are monitored by using IR, and the presence of significant amounts of $[Fe_3Pt_3(CO)_{15}]^{\cdot-}$ and $[EtV]^{\cdot+}$ in the reaction solution has been confirmed by using EPR spectroscopy. The primary presence of bis-charged anions and cations in the crystals can be explained in two ways. Firstly, by assuming a much greater insolubility of the 2+/2− with respect to the 1+/1− salt, which causes a back-shift of the equilibrium in Equation (3) owing to precipitation of the 2+/2− salt. Secondly, an electron transfer in the solid state, also corresponding to a back-shift of equilibrium in Equation (3), driven by the gain in lattice energy of a 2+/2− salt.

The EPR spectrum of the $[EtV][Fe_3Pt_3(CO)_{15}]\cdot THF$ salt: The crystals the $[EtV][Fe_3Pt_3(CO)_{15}]\cdot THF$ salt are soluble in THF, acetone and acetonitrile and give rise to deep-blue solutions. The IR spectrum of these solutions shows the carbonyl infrared absorptions expected for a $[Fe_3Pt_3(CO)_{15}]^{2-/\cdot-}$ mixture. The IR frequencies and patterns are coincident with those of corresponding tetrasubstituted ammonium

salts. The concomitant EPR spectrum of these solutions discloses the presence of rather intense signals of $[Fe_3Pt_3(CO)_{15}]^{\bullet-}$ and $[EtV]^{\bullet+}$ in a ≈1:1 ratio (Figure 5a), in keeping with occurrence of the equilibrium in Equation (3). In partial contrast, the EPR spectrum of a microcrystalline sample shows a broad isotropic signal, which might be a result of coupling/exchange broadening of the above signals (Figure 5b). Its relatively low intensity is in keeping (qualitative) with a retro-shift of the equilibrium in Equation (3) in the solid state, with respect to solution.

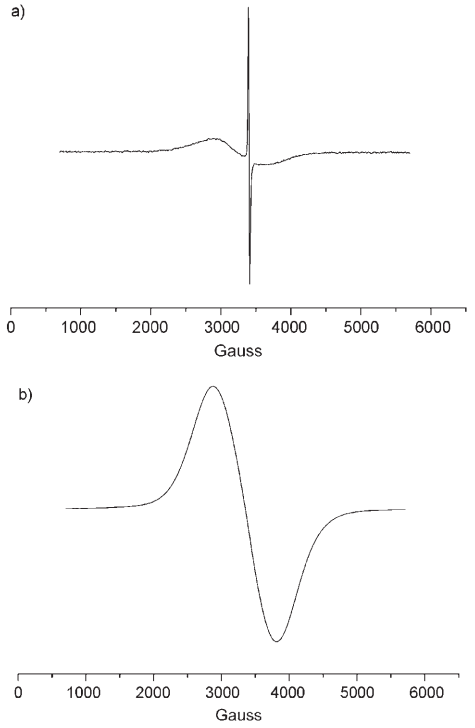

Figure 5. The EPR spectra of $[EtV][Fe_3Pt_3(CO)_{15}]\cdot THF$ a) in acetonitrile and b) in a solid microcrystalline state.

The structure of the $[EtV][Fe_4Au(CO)_{16}]_2\cdot 2THF$ and $[NEt_4][Fe_4Au(CO)_{16}]$ salts: The crystal packing of $[EtV][Fe_4Au(CO)_{16}]_2\cdot 2THF$ does not display any particular feature, having all the ions separated by normal ionic distances. However, the structure of the $[Fe_4Au(CO)_{16}]^-$ ion (Figure 6) presents a significant novelty with respect to the previously reported structure of the salt $[NMe_3CH_2Ph]_2[Fe_4Au(CO)_{16}]Cl$.[14,15] In $[NMe_3CH_2Ph]_2[Fe_4Au(CO)_{16}]Cl$, the two $Fe_2(CO)_8$ moieties that give rise to a square-planar coordination around the gold atom, only contain terminal carbonyl groups. Whereas in $[EtV][Fe_4Au(CO)_{16}]_2\cdot 2THF$, one of the $Fe_2(CO)_8$ moieties features two slightly asymmetric bridging CO ligands (Fe–C_{av} 1.94–2.05 Å; Fe–C–O angle 136.2–143.5°) and, thus, it should be more precisely written as $[Fe_4Au(CO)_{14}(\mu\text{-}CO)_2]^-$. Moreover, one CO ligand per Fe atom in the all terminal $Fe_2(CO)_8$ group is bent toward the central Au atom [Au–C 2.79 Å], probably as a result of non-bonding C···C repulsions around the Fe centres and attraction from the formally Au^{III} central ion.

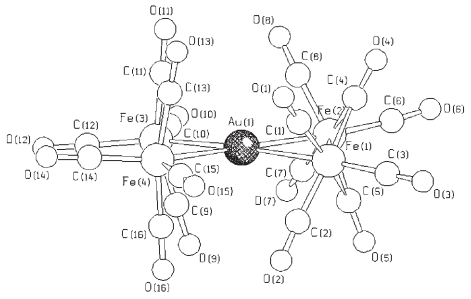

Figure 6. The structure of the $[Fe_4Au(CO)_{16}]^-$ ion present in both the $[EtV][Fe_4Au(CO)_{16}]_2\cdot 2THF$ and $[NEt_4][Fe_4Au(CO)_{16}]$ salts.

The reason why two different isomers, $[Fe_4Au(CO)_{16}]^-$ and $[Fe_4Au(CO)_{14}(\mu\text{-}CO)_2]^-$, are present in the $[NMe_3CH_2Ph]_2[Fe_4Au(CO)_{16}]Cl$ and $[EtV][Fe_4Au(CO)_{16}]_2\cdot 2THF$ salts is not straightforward. Both salts dissolve in organic solvents and display identical IR spectra that mainly features $\tilde{\nu}_{CO}$ characteristics that are ascribed to terminal CO ligands and only very weak absorptions attributable to bridging carbonyl groups. On the basis of their relative intensities, it can be roughly inferred that the equilibrium constant for the interconversion in Equation (5) in solution of the two isomers is $\approx\times 10^{-1}$ to $\times 10^{-2}$.

$$[Fe_4Au(CO)_{16}]^- \rightleftharpoons [Fe_4Au(CO)_{14}(\mu\text{-}CO)_2]^- \quad (5)$$

Nonetheless, upon crystallization of $[EtV][Fe_4Au(CO)_{16}]_2\cdot 2THF$, the equilibrium is shifted toward the minor isomer. The particular cation of the salt, as well as any CT or ET process between anions and cations, does not play any role in the isomerization. Indeed, a completely identical structure of the anion has been ascertained, also in the $[NEt_4][Fe_4Au(CO)_{16}]$ salt (Table 4). The most likely conclusion is that the isomerization process upon crystallization is determined by packing effects. Thus, the crystals of $[EtV][Fe_4Au(CO)_{16}]_2\cdot 2THF$ and $[NEt_4][Fe_4Au(CO)_{16}]$, even though they have different stoichiometries, present very similar densities of 2.021 and 2.023 $g\,cm^{-3}$, respectively. In contrast, $[NMe_3CH_2Ph]_2[Fe_4Au(CO)_{16}]Cl$ is considerably less dense (1.760 $g\,cm^{-3}$). Isomerization of $[Fe_4Au(CO)_{16}]^-$ into $[Fe_4Au(CO)_{14}(\mu\text{-}CO)_2]^-$ results in a decreased volume of the anion, because of significant shortening of the CO support-

Table 4. Comparison between the bond lengths [Å] in $[NMe_3CH_2Ph]_2[Fe_4Au(CO)_{16}]Cl$, $[NEt_4][Fe_4Au(CO)_{16}]$ and $[EtV][Fe_4Au(CO)_{16}]_2\cdot 2THF$.

	$[NMe_3CH_2Ph]_2[Fe_4Au(CO)_{16}]Cl$	$[NEt_4][Fe_4Au(CO)_{16}]$	$[EtV][Fe_4Au(CO)_{16}]_2\cdot 2THF$
Au–Fe	2.583	2.590	2.588
	2.607	2.599	2.620
Fe–Fe[a]	2.771	2.765	2.764
Fe–Fe[b]	–	2.574	2.571

[a] All terminal CO. [b] Including bridging CO.

ed Fe–Fe interaction. It appears, therefore, conceivable to suggest that the more compact packing of [EtV]-$[Fe_4Au(CO)_{16}]_2$·2THF and $[NEt_4][Fe_4Au(CO)_{16}]$ shifts the equilibrium in Equation (5) towards the right, whereas the less compact packing, a result of the 1:1 cocrystallization of $[NMe_3CH_2Ph][Fe_4Au(CO)_{16}]$ and $[NMe_3CH_2Ph]Cl$, keeps the equilibrium shifted to the left.

In agreement with their solid-state structures, the IR spectra in nujol mull of both $[EtV][Fe_4Au(CO)_{16}]_2$·2THF and $[NEt_4][Fe_4Au(CO)_{16}]$, display intense stretching bands at 1815 and 1784 cm^{-1} (bridging CO ligands) that are considerably stronger than in solution, which are completely absent in the nujol mull IR spectrum of $[NMe_3CH_2Ph]_2$-$[Fe_4Au(CO)_{16}]Cl$.

It is widely accepted that energy barrier for the terminal-bridge interconversion of the CO ligands is low, as deduced from the easy scrambling processes of several carbonyl compounds on the ^{13}C NMR timescale.[30] It is now shown that such interconversion can be promoted by packing forces.

Resistivity measurements: Of the three ethylviologen salt structures described here, two of them, [EtV]-$[Fe_3Pt_3(CO)_{15}]$·THF and $[EtV][Fe_4Au(CO)_{16}]_2$·2THF, can be described as purely ionic, in the sense that all ions are near completely isolated and do not give rise to suprastructures, as observed for $[EtV]^{\bullet+}[HFe_3(CO)_{11}]$, $[(EtV)^{\bullet+}]_5$-$[Ag_{13}Fe_8(CO)_{32}]$[5] and $[MeV]^{\bullet+}[PF_6]$[17] salts. The structure of $[EtV]_2[Fe_4Pt(CO)_{16}]$ is exceptional in that it features the presence of infinite stacks of twisted and tilted $[(EtV)^{\bullet+}]_2$ π-dimers. All of these salts contain cations and anions, which are redox active with ΔE in the 0–0.4 V range. Such a range of values is often thought to be the optimum for ΔE to give rise to $D^{\delta+}-A^{\delta-}$ CT or ET phenomena. For this reason, the electrical properties of these materials as pressed pellets have been investigated by means of a standard 4-point probe. For the sake of comparison, also the resistivity of $[NMe_3CH_2Ph]_2[Fe_3Pt_3(CO)_{15}]$, $[NMe_3CH_2Ph]_2[Fe_4Pt(CO)_{16}]$ and $[NMe_3CH_2Ph]_2[Fe_4Au(CO)_{16}]Cl$ has been measured and the results are collated in Table 5.

The data clearly show that both the $[Fe_4Au(CO)_{16}]^-$ salts are insulators with a resistivity so high that a reliable measure was beyond our equipment, whereas for the other compounds it has been possible to measure a reproducible resistivity. For both salts based on $[Fe_3Pt_3(CO)_{15}]^{2-}$ and $[Fe_4Pt(CO)_{16}]^{2-}$, a significant decrease of the resistivity of 3–4 orders of magnitude is observed on passing from the non-redox-active $[NMe_3CH_2Ph]^+$ ion to the redox-active ethylviologen. Significantly, the lowest resistivity is displayed by the $[EtV][Fe_3Pt_3(CO)_{15}]$·THF salt, in which the redox couples of the cation and the anion exhibit a ΔE of ≈ 0 V in solution. Such a low resistivity indicts a certain degree of ET behaviour between anion and cation also in the solid state and is in keeping with the observation of the EPR signals of $[EtV]^{\bullet+}$ and $[Fe_3Pt_3(CO)_{15}]^{\bullet-}$ in crystalline samples of [EtV]-$[Fe_3Pt_3(CO)_{15}]$·THF. Apparently, the ET process becomes almost negligible as the ΔE increases to 0.4 V (e.g., $[EtV]_2$-$[Fe_4Pt(CO)_{16}]$) and is completely absent in [EtV]-$[Fe_4Au(CO)_{16}]_2$·2THF, in which the anion is already in its highest possible oxidation state being formally a square planar complex of Au^{III}, rather than Pt^{II}, of the $[Fe_2(CO)_8]^{2-}$ bidentate ligand.

Table 5. Resistivities for the viologen and tetra-alkylammonium salts of the mixed metal clusters studied.

Compound	ρ [Ω cm]
$[NMe_3CH_2Ph]_2[Fe_3Pt_3(CO)_{15}]$	1.5×10^{8}
$[EtV][Fe_3Pt_3(CO)_{15}]$·THF	6.6×10^{4}
$[NMe_3CH_2Ph]_2[Fe_4Pt(CO)_{16}]$	3.8×10^{9}
$[EtV]_2[Fe_4Pt(CO)_{16}]$	4.6×10^{6}
$[NMe_3CH_2Ph]_2[Fe_4Au(CO)_{16}]Cl$	[a]
$[EtV][Fe_4Au(CO)_{16}]_2$·2THF	[a]

[a] The ρ was too high to be measured accurately.

Conclusion

As a major bonus of the preparation and characterization of the $[(EtV)^{\bullet+}]_2[Fe_4Pt(CO)_{16}]$, $[EtV][Fe_3Pt_3(CO)_{15}]$·THF and $[EtV][Fe_4Au(CO)_{16}]_2$·2THF hybrid salts, we have isolated and structurally characterized for the first time an example of a long-bonded π-dimer of the $[EtV]^{\bullet+}$ radical ion and demonstrated that such interactions can give rise to a significantly populated triplet state, detectable by solid-state EPR spectroscopy. Moreover, it has been shown that packing forces may significantly alter not only the carbonyl stereochemistry of a given carbonyl cluster, by shifting isomerization equilibrium one or the other way, but can also shift the redox equilibrium in solution.

As far as conductivity of the above hybrid salts is concerned, it can be concluded that their resistivity as pellets is not exciting and most behave as insulators. However, at least $[EtV][Fe_3Pt_3(CO)_{15}]$·THF can be classified as a semiconductor. The semiconductor characteristics may stem from the presence of $[EtV]^{2+}$ and $[Fe_3Pt_3(CO)_{15}]^{2-}$ interionic, loose interactions in the crystalline state. However, these sub van der Waals contacts are not enough to enable efficient electron transfer in the material. Nonetheless, the conductivity of the latter is 3–4 orders of magnitude greater than that of stoichiometric salts of viologen dications and monocations with inorganic counterions ($\times10^{-7}$ to $\times10^{-10}$ $S\,cm^{-1}$; the highest values are attributed to the presence of stacks of viologen monocations), and approaches the conductivity of mixed-valent p-cyanophenyl disubstituted viologens ($\times10^{-5}$ $S\,cm^{-1}$) exhibiting stoichiometries such as $[RV^{2+}][RV^{\bullet+}]_2[BF_4]_4$.(R=*p*-cyanophenyl)[4] A similar situation holds for stoichiometric crystalline (TTF)X and $(TTF)X_2$ (X = Cl, Br, I; TTF = tetrathiafulvalene) salts, which contains $(TTF^{\bullet+})_2$ dimers, whereas the nonstoichiometric $(TTF)X_n$ ($n = 0.59$–079) ordered or disordered mixed-valence phases display a 6–7 order of magnitude greater conductivity.[31] Attempts to improve the conductivity of the above hybrid materials by variation of the viologen substituents are in progress.

Experimental Section

All reactions and sample manipulations were carried out by using standard Schlenk techniques under nitrogen and in dried solvents. The M_2-$[Fe_3Pt_3(CO)_{15}]$, $M_2[Fe_4Pt(CO)_{16}]$ and $M[Fe_4Au(CO)_{16}]$ (M = Na, K) salts have been prepared according to the literature.[6,8,14] Analysis of Fe, Pt and Au were performed by using atomic absorption on a Pye-Unicam instrument. Analyses of C, H and N were obtained with a ThermoQuest FlashEA 1112NC instrument. IR spectra were recorded on a Perkin–Elmer SpectrumOne interferometer in CaF_2 cells. EPR spectra have been recorded by using a Bruker ESP300E spectrometer. The simulation of the EPR spectrum in Figure 3b was performed by means of commercial Bruker software XSophe. The figures were drawn with SCHAKAL99.[32] Resistivity measurements were performed by using a Keithley 2400 SourceMeter equipped with a 4-point probe, using polycrystalline materials pressed into pellets of diameter $\approx$13 mm and thickness $\approx$1 mm.

Synthesis of [EtV][$Fe_3Pt_3(CO)_{15}$]·THF: A suspension of $[EtV]I_2$ (0.60 g, 1.28 mmol) in methanol (20 mL) was added to $Na_2[Fe_3Pt_3(CO)_{15}]$ (1.1 g, 0.90 mmol) dissolved in MeOH (20 mL), until complete precipitation of the cluster was observed. The solid was filtered, washed with water (3× 10 mL) and extracted into THF (20 mL). Crystals of [EtV]-$[Fe_3Pt_3(CO)_{15}]$·THF suitable for X-ray analysis were obtained by slow diffusion of toluene on this solution (yield 1.04 g, 79%). The salt is soluble in THF, acetone, acetonitrile, DMF, DMSO, sparingly soluble in alcohols and insoluble in nonpolar solvents. Elemental analysis calcd (%) for $C_{33}H_{26}Fe_3N_2O_{16}Pt_3$: C 27.1, H 1.80, N 1.92, Fe 11.49, Pt, 40.10; found: C 27.3 , H 1.90, N 1.91, Fe 11.35, Pt 39.98.

Synthesis of [EtV]$_2$[$Fe_4Pt(CO)_{16}$]: A solution of $[EtV]I_2$ (0.51 g, 1.09 mmol) in methanol (40 mL) was added to $Na_2[Fe_4Pt(CO)_{16}]$ (0.88 g, 0.96 mmol) dissolved in methanol (20 mL), until complete precipitation of the cluster was observed. The solid was filtered, washed with water (2×20 mL) and extracted into acetone (30 mL). Crystals of $[EtV]_2$-$[Fe_4Pt(CO)_{16}]$ suitable for X-ray analysis were obtained by slow diffusion of isopropyl alcohol into this solution (yield 1.05 g, 84.5%). The salt is soluble in acetone, acetonitrile, DMF, DMSO, sparingly soluble in THF and alcohols and insoluble in non-polar solvents. Elemental analysis calcd (%) for $C_{44}H_{36}Fe_4N_4O_{16}Pt$: C 40.8, H 2.8, N 4.3, Fe 17.3, Pt 15.1; found: C 40.6 , H 2.83 , N 4.15, Fe 17.1 , Pt 15.0.

Synthesis of [EtV][$Fe_4Au(CO)_{16}$]$_2$·2THF: A suspension of $[EtV]I_2$ (0.62 g, 1.32 mmol) in methanol (20 mL) was added to $K[Fe_4Au(CO)_{16}]$ (0.77 g, 0.85 mmol) dissolved in MeOH (20 mL), until complete precipitation of the cluster was observed. The solid was filtered off, washed with water (3×15 mL) and extracted into THF (20 mL). Crystals of [EtV]-$[Fe_4Au(CO)_{16}]_2$·2THF suitable for X-ray analysis were obtained by slow diffusion of toluene on this solution (yield . 0.85 g, 85%). The salt is soluble in THF, acetone, acetonitrile, DMF, DMSO, sparingly soluble in alcohols and insoluble in non-polar solvents. Elemental analysis calcd (%) for $C_{54}H_{34}Au_2Fe_8N_2O_{34}$: C 35.3, H 2.25, N 2.40, Fe 19.35, Au 17.1; found: C 35.1, H 2.21, N 2.28, Fe 19.15, Au 16.95.

X-ray studies: Crystal data and collection details for [EtV]-$[Fe_3Pt_3(CO)_{15}]$·THF, $[EtV]_2[Fe_4Pt(CO)_{16}]$, $[EtV][Fe_4Au(CO)_{16}]_2$·2THF and $[NEt_4][Fe_4Au(CO)_{16}]$ are reported in Table 6. The diffraction experiments were carried out on a Bruker APEX II diffractometer equipped with a CCD detector using $Mo_{K\alpha}$ radiation. Data were corrected for Lorentz polarization and absorption effects (empirical absorption correction SADABS).[33] Structures were solved by using direct methods and refined by means of full-matrix least-squares based on all data using F^2.[34] Hydrogen atoms were fixed at calculated positions and refined by using a riding model. All nonhydrogen atoms were refined with anisotropic displacement parameters.

CCDC 639144–639149 contains the supplementary crystallographic data for this paper. These data can be obtained free of charge from the Cambridge Crystallographic Data Centre via ww.ccdc.cam.ac.uk/data_request.cif.

Table 6. Crystal data and experimental details for [EtV][$Fe_3Pt_3(CO)_{15}$]·THF, $[EtV]_2[Fe_4Pt(CO)_{16}]$, $[EtV][Fe_4Au(CO)_{16}]_2$·2THF and $[NEt_4][Fe_4Au(CO)_{16}]$.

	[EtV][$Fe_3Pt_3(CO)_{15}$]·THF	$[EtV]_2[Fe_4Pt(CO)_{16}]$	$[EtV][Fe_4Au(CO)_{16}]_2$·2THF	$[NEt_4]$ $[Fe_4Au(CO)_{16}]$
formula	$C_{33}H_{26}Fe_3N_2O_{16}Pt_3$	$C_{44}H_{36}Fe_4N_4O_{16}Pt$	$C_{54}H_{34}Au_2Fe_8N_2O_{34}$	$C_{24}H_{20}AuFe_4NO_{16}$
M_r	1459.38	1295.26	1047.78	998.78
T [K]	100(2)	100(2)	296(2)	295(2)
λ [Å]	0.71073	0.71073	0.71073	0.71073
crystal system	monoclinic	monoclinic	monoclinic	monoclinic
space group	$P2_1/c$	$C2/c$	$P2_1/c$	$P2_1/n$
a [Å]	10.0555(10)	14.741(2)	15.397(2)	13.5548(17)
b [Å]	9.8220(10)	22.361(4)	12.0809(2)	16.781(2)
c [Å]	39.477(4)	14.306(2)	19.807(	14.4184(18)
α [°]	90	90	90	90
β [°]	90.301	99.351(2)	110.855(2)	91.399(2)
γ [°]	90	90	90	90
V [Å^3]	3898.9(7)	4653(6)	3442.9(8)	3278.6(7)
Z	4	4	2	4
δ_{calcd} [g cm^{-3}]	2.486	1.849	2.021	2.023
μ [mm^{-1}]	11.883	4.289	5.966	6.257
F(000)	2712	2552	2020	1928
crystal size [mm]	0.20×0.15×0.10	0.25×0.20×0.15	0.22×0.16×0.12	0.22×0.18×0.14
θ limits [°]	2.03–25.00	1.67–25.00	1.42–26.00	1.86–27.00
index ranges	$-11 \le h \le 11$	$-17 \le h \le 17$	$-18 \le h \le 18$	$-17 \le h \le 17$
	$-11 \le k \le 11$	$-26 \le k \le 26$	$-14 \le k \le 14$	$-21 \le k \le 21$
	$-46 \le l \le 46$	$-17 \le l \le 17$	$-24 \le l \le 24$	$-18 \le l \le 18$
reflections collected	34934	21446	34640	35746
independent reflections	6862 [R(int) = 0.0274]	4102 [R(int) = 0.0614]	6749 [R(int) = 0.0441]	7167 [R(int) = 0.0360]
completeness to θ = 25.00° [%]	100.0	100.0	100.0	100.0
data/restraints/parameters	6862/102/516	4102/0/314	6749/56/452	7167/41/408
goodness of fit on F^2	1.385	1.014	1.032	1.017
R_1 [$I > 2\sigma(I)$]	0.0394	0.0259	0.0237	0.0244
wR_2 (all data)	0.0720	0.0633	0.0581	0.0591
largest diff. peak/hole [e Å^{-3}]	2.203/−2.400	0.731/−0.977	0.544/−0.537	0.488/−0.474

Acknowledgements

The financial contribution of PRITT2004 and PRIN2006 is gratefully acknowledged.

[1] P. Cassoux, J. L. Miller in *Chemistry of Advanced Materials: An Overview*, (Eds.: L. V. Interrante, M. J. Hampden-Smith), Wiley-VCH, Weinheim, **1998**, 19–59, and references therein.
[2] G. Longoni, C. Femoni, M. C. Iapalucci, P. Zanello, in *Metal Clusters in Chemistry*, (Eds.: P. Braunstein, L. Oro, P. Raithby), Wiley-VCH, Weinheim, **1999**, 1137–1158.
[3] C. Femoni, F. Kaswalder, M. C. Iapalucci, G. Longoni, S. Zacchini, *Coord. Chem. Rev.* **2006**, *250*, 1580–1604.
[4] P. M. S. Monk, *The Viologens*, J. Wiley and Sons, Chichester, **1998**, and references therein.
[5] D. Collini, C. Femoni, M. C. Iapalucci, G. Longoni, *Compt. Rend. Chim.* **2005**, *8*, 1645–1654.
[6] G. Longoni, M. Manassero, M. Sansoni, *J. Am. Chem. Soc.* **1980**, *102*, 3242–3244.
[7] P. Zanello, *Struct. Bond.* **1992**, *79*, 101–214.
[8] G. Longoni, M. Manassero, M. Sansoni, *J. Am. Chem. Soc.* **1980**, *102*, 7973–7975.
[9] P. J. Kruzic, J. San Filippo, B. Hutchinson, R. L. Hance, L. M. Daniels, *J. Am. Chem. Soc.* **1981**, *103*, 2129–2131.
[10] F. Ragaini, D. L. Ramage, J-S. Song, G. L. Geoffroy, A. L. Rheingold, *J. Am. Chem. Soc.* **1993**, *115*, 12183–12184.
[11] G. Longoni, P. Chini, *J. Am. Chem. Soc.* **1976**, *98*, 7225–7231.
[12] L. F. Dahl, J. F. Blount, *Inorg. Chem.* **1965**, *4*, 1373–1375.
[13] R. Della Pergola, L. Garlaschelli, C. Mealli, D. M. Proserpio, P. Zanello, *J. Cluster Sci.* **1990**, *1*, 93–106.
[14] V. G. Albano, R. Aureli, M. C. Iapalucci, F. Laschi, G. Longoni, M. Monari, P. Zanello, *J. Chem. Soc. Chem. Commun.* **1993**, 1501–1502.
[15] V. G. Albano, F. Demartin, C. Femoni, M. C. Iapalucci, G. Longoni, P. Macchi, M. Monari, *Solid State Sci.* **1999**, *1*, 597–606.
[16] J.-M. Lü, S. V. Rosokha, J. K. Kochi, *J. Am. Chem. Soc.* **2003**, *125*, 12161–12171.
[17] W. S. Jeon, H.-J. Kim, C. Lee, K. Kim, *Chem. Commun.* **2002**, 1828–1829.
[18] T. M. Bockman, J. K. Kochi, *J. Org. Chem.* **1990**, *55*, 4127–4135.
[19] P. Chini, *Inorg. Chim. Acta Rev.* **1968**, 31–51.
[20] T. Stanley Cameron, A. Decken, R. M. Kowalczyk, E. J. L. McInnes, J. Passmore, J. M. Rawson, K. V. Shuvaev, L. K. Thompson, *Chem. Commun.* **2006**, 2277–2279.
[21] J. Hermolin, M. Levin, Y. Ikegami, M. Sawayanagi, E. M. Kosower, *J. Am. Chem. Soc.* **1981**, *103*, 4795–4800.
[22] J. R. Gee, W. A. Howard, G. L. McPherson, M. J. Fink, *J. Am. Chem. Soc.* **1991**, *113*, 5461–5462.
[23] P. Dowd, Y. H. Paik, *J. Am. Chem. Soc.* **1986**, *108*, 2788–2790.
[24] A. Ito, Y. Ono, K. Tanaka, *Angew. Chem.* **2000**, *112*,1114–1117; *Angew. Chem. Int. Ed.* **2000**, *39*, 1072–1075.
[25] B. D. Koivisto, A. S. Ichimura, R. McDonald, M. T. Lemaire, L. K. Thompson, R. J. Hicks, *J. Am. Chem. Soc.* **2006**, *128*, 690–691.
[26] R. D. Adams, A. Arafa, G. Chen, J. C. Lii, J. G. Wang, *Organometallics* **1990**, *9*, 2350–2357.
[27] H. J. Hofmann, R. Cimiraglia, J. Tomasi, *J. Mol. Struct. THEOCHEM* **1986**, *139*, 213–219.
[28] H. J. Hofmann, R. Cimiraglia, J. Tomasi, *J. Chem. Soc. Chem. Res.*, *Synop* **1987**, 48–49.
[29] A. L. Gillon, G. R. Lewis, A. G. Orpen, S. Rotter, J. Starbuck, X-M. Wang, Y. Rodriguez-Martin, C. Ruiz-Perez, *J. Chem. Soc., Dalton Trans.* **2000**, 3897–3905.
[30] E. Band, E. L. Muetterties, *Chem. Rev.* **1978**, *78*, 639–657.
[31] B. A. Scott, S. J. La Placa, J. B. Torrance, B. D. Silverman, B. Welber, *J. Am. Chem. Soc.* **1977**, *99*, 6631–6639.
[32] E. Keller, SCHAKAL99, University of Freiburg, Germany, **1999**.
[33] G. M. Sheldrick, SADABS, University of Gottingen, Germany, **1996**.
[34] G. M. Sheldrick, SHELX97, University of Gottingen, Germany.

Received: March 9, 2007
Published online: July 5, 2007

